11-13 November 2025
Vol 27, pp.67-82 Proceedings Book "Bangkok Conference - Thailand" 10.051103/PBS.251227708

Toward Human-Like Manipulation: A Dexterous Robotic Hand for Complex Grasping Tasks with Real-Time Control via Flex Sensor-based Glove

Natthapol Sriratanasak [#1], Pisak Chermprayong [#2*], Mattana Santasnachok [#3], Ekkachai Sutheerasak[#4]

[#] *Department of Mechanical Engineering, Faculty of Engineering, Burapha University, Chonburi, 20131, Thailand*

[1]natthapol.sr@eng.buu.ac.th

[2]pisak.ch@eng.buu.ac.th

[3]mattana@eng.buu.ac.th

[4]ekkachai@eng.buu.ac.th

**corresponding author*

Abstract—**Developing robotic hands capable of manipulating objects and tools remains a significant challenge due to the requirement of effective coordinated finger articulation and palm compliance. This study presents the design and development of a dexterous robotic hand capable of executing complex grasping and manipulation tasks through real-time teleoperation using a custom glove embedded with flex sensors. The proposed robotic hand features 15 active degrees of freedom and employs a tendon-driven mechanism to enable natural, human-like finger movements. Built upon the open-source DexHand V1 platform, the robotic hand incorporates multi-degree-of-freedom joints and a silicone-coated exterior to enhance grip compliance and friction. A teleoperation glove equipped with nine flex sensors was developed to allow intuitive and responsive control of the robotic hand. Kinematic analysis of the mechanism is presented, and sensor performance was evaluated under both static and dynamic conditions, demonstrating stable and repeatable readings. Experimental results show that the robotic hand successfully replicates complex finger motions and performs a variety of tasks, including grasping spherical objects, executing precision grips (e.g., holding a needle), lifting heavy items (up to 2.1 kg, such as a hammer), and performing in-hand manipulations. In conclusion, the integration of human-centred design and intuitive control strategies enables the robotic hand to closely emulate human grasping behaviour, highlighting its potential for applications in teleoperation, assistive technology, and service robotics.**

Keywords—**Anthropomorphic Design, Dexterous Robotic Hand, Flex Sensor-Based Control, Object Manipulation, Real-Time Teleoperation**

I. INTRODUCTION

In human environments, grasping and manipulating a diverse range of objects—varying in shape, size, weight, and surface texture—are tasks performed effortlessly by the human hand. This exceptional capability arises from its complex musculoskeletal structure, comprising 38 compliant actuators distributed across the fingers, palm, and wrist [1], and enhanced by frictional characteristics provided by fingerprints [2]. Replicating this level of dexterity and adaptability remains one of the most formidable challenges in robotics.

Over the past few decades, the development of anthropomorphic robotic hands has been a significant focus in the robotics research community. The goal is to create systems capable of performing human-like manipulation in unstructured and dynamic environments. A wide range of mechanical architectures and control strategies have been proposed to emulate the dexterity, compliance, and sensory integration of the human hand. Among these, motor-driven designs have emerged as the predominant approach [3], broadly classified into motor-direct-driven, linkage-driven, and tendon-driven mechanisms [4].

Motor-direct-driven mechanisms utilize actuators directly coupled to the joints via gears, pulleys, or linkages [5], [6]. These designs enable precise position and torque control, making them suitable for tasks requiring strong and stable grasps. However, the trade-offs include increased weight, reduced dexterity, and mechanical complexity due to motor placement within or near each joint.

ISSN: 2961-6611

Linkage-driven mechanisms offer compact actuation by transmitting motor power through mechanical linkages to multiple joints [7], [8]. This method enables efficient motion transmission and bidirectional control of fingers [9], but limits dexterity due to rigid mechanical structures and vulnerability at joint pivots. Notably, Kim et al. [10] demonstrated a highly functional linkage-driven hand capable of executing delicate tasks, such as using scissors and tweezers—highlighting the potential of this architecture.

Tendon-driven mechanisms have gained prominence as the most biologically inspired solution. These systems replicate the anatomy of human tendons, with cables routed through the phalanges and actuated remotely by motors located in the palm or forearm [11], [12]. This design minimizes on-hand weight, allows for compact finger design, and can achieve high fingertip forces. Moreover, tendon-driven hands facilitate more human-like movement patterns, including grasp adaptation and fine in-hand manipulation.

Despite mechanical advancements, a critical barrier remains in the control of robotic hands during dynamic and uncertain interactions with real-world objects. While grasping canonical geometric shapes (e.g., spheres, cylinders, cuboids) can be achieved through open-loop or model-based control strategies [13], robust manipulation of irregular, deformable, or task-specific objects requires human-in-the-loop control, real-time adaptation, and sensor integration.

Recent trends focus on real-time control (RTC) systems that map human hand movements directly to robotic hands using wearable devices or vision-based tracking. Prominent techniques include flex sensor-based data gloves [14], [15], offering low-latency finger tracking, and vision systems using RGB or depth cameras with AI-driven pose estimation [16], [17]. These approaches enable more intuitive teleoperation, allowing robotic systems to leverage the user's motor intelligence and adapt to novel manipulation contexts.

Although robotic hands can be designed to resemble the human hand and mimic its behaviour, significant research challenges remain in grasping and manipulating objects [18]. These challenges include:

i) Grasping objects with narrow or curved surfaces which require precise contact points for stability.
ii) Regrasping – where an object is picked up with one grasp but needs to be repositioned for further manipulation.
iii) Task-specific grasping – holding an object in a specific way for its intended function.
iv) In-hand manipulation – where the robotic hand must not only grasp but also manipulate the object simultaneously.

Much of the progress to date has focused on finger design and individual joint actuation, often overlooking the essential role of palm compliance and wrist dynamics in human-like object handling. Grasping is inherently a whole-hand activity, requiring coordinated control of all degrees of freedom to manage object inertia, centre of mass, and task constraints.

To address these limitations, this study presents a dexterous, linkage-driven robotic hand developed on the open-source DexHand V1 platform [19]. DexHand provides a highly modular, human-scale design with kinematics resembling a human hand. Our system integrates a robotic hand with linkage-driven mechanism enabling bi-directional control of individual fingers, a flex sensor-based glove for real-time teleoperation, and a silicone-rubber-coated palm and fingers to improve compliance and grip adaptability. As illustrated in Fig. 1(a–c), the complete system includes the robotic hand and forearm, control electronics, and a wearable glove interface. The glove captures human finger movements in real time and translates them into robotic joint commands. Comprehensive experiments were conducted to validate the hand's performance in real-world scenarios, including grasping basic shapes and household items, fine manipulation of small tools such as needles and wire strippers, and handling of heavy, irregular objects such as a 2.1 kg hammer. The robotic hand demonstrated capabilities beyond traditional grasping, including fingertip coordination, palm-supported grips, and in-hand object manipulation—closely mimicking human manipulation strategies.

The remaining of the paper is organised as followed. Section II describes the design and kinematic model of the proposed robotic hand. The control architecture of the flex sensor-based glove is also presented in this section. Following that, Section III presents the performance evaluation of the developed system including finger motion, static and dynamics performance of the glove and demonstration of the robotic system to grasp and manipulate several objects and tools. Finally, Section IV gives the conclusion of this work.

ISSN: 2961-6611

Vol 27, pp.67-82 Proceedings Book "Bangkok Conference - Thailand" 10.051103/PBS.251227708

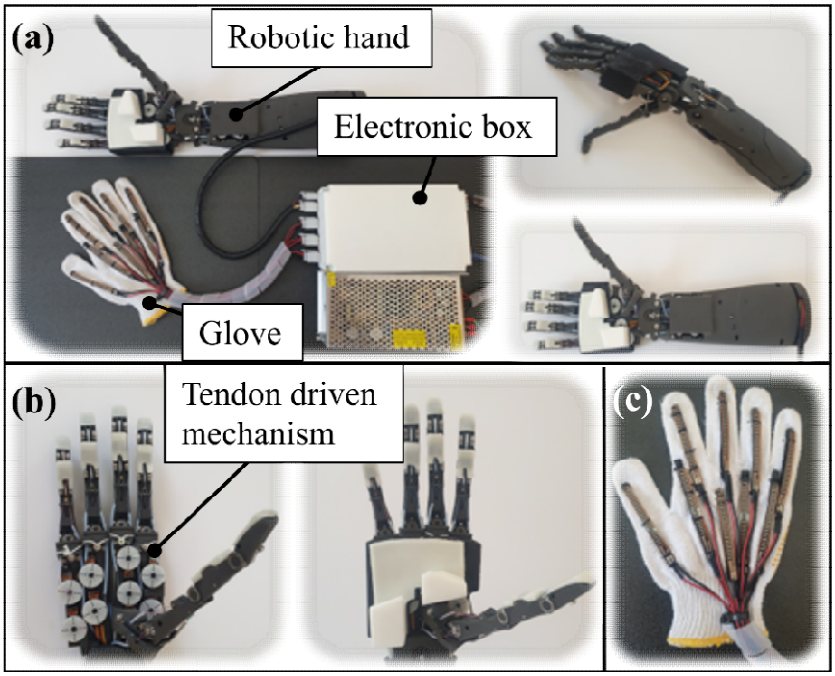

Fig. 1 Overview of the robotic hand. (a) Integration of robotic hand, electronic box and RTC glove. (b) Robotic hand (left) with and (right) without silicone cover to enhance object grasping. (c) The glove based of flex sensor for real-time control.

II. Robotic Hand System

A. Design of The Robotic Hand

The robotic hand consists of palm, five fingers, and forearm. All components are fabricated using Nylon 12 through Selective Laser Sintering (SLS) 3D printing. As shown in Fig. 2(a), each finger consists of three segments: fingertip (distal phalanx-DP), middle phalanx (MP) and proximal phalanx (PP) connecting to a palm. All joints connecting these segments are constructed using two bearings per joint, with joint axes aligned along the axial axes of the bearings. This configuration provides low-friction revolute joints, enhancing smooth finger articulation. Furthermore, the fingertip-MP joint and MP-PP joint each have 1 DOF. The joint connecting between PP and palm sections replicates metacarpophalangeal (MCP) joint of human finger providing 2 DOFs and allowing greater flexibility as shown in Fig. 2(b). These 2 DOFs are controlled by primary and secondary joints. Among all five fingers, the thumb plays the most crucial role in grasping and manipulating objects, as it provides most of the grasping force and helps orient objects to match the hand's shape [20]. Hence, the joint connecting between PP and palm sections of the thumb is designed to replicate the carpometacarpal (CMC) joint of a human thumb as shown in Fig. 2(c). The CMC joint has 3 DOFs with ad additional tertiary joint. In summary, the DexHand V1, including five fingers has 15 DOFs comprising of 21 joints (15 active and 6 passive joints).

Each finger has three cables: one cables are pinned at the fingertip and the remaining two cables are pins at the middle of PP sections. Fingertip, MP, PP and palm are pressed against the outer surface of bearings by tension of these cables. Each end of cable is individually connected to servo motor thus providing 3 controllable DOFs. All 15 active joints are powered by 15 servo motors, with 8 motors positioned in the palm and the remaining 7 housed in the forearm. Thus, each finger can perform the full range of human finger movements, including extension-flexion, abduction-adduction, and circumduction [21]. The original design of DexHand V1 provides additional 2 DOFs of the wrist as well but it is excluded in this study.

Each finger is controlled by three servo motors using a tendon-driven mechanism, as illustrated in Fig. 2(d). *Cable 1* is anchored at the fingertip and routed through slots within the metacarpal phalange (MP), proximal phalange (PP), palm and wrist before connecting to *Servo Motor 1* (*Servo 1*) in the forearm. When *Servo1* activates, it pulls *Cable 1*, making the fingertip-PP joint an active joint, thereby generating flexion movement in both the fingertip and MP sections of the finger. To enable extension, *Cable 2* is anchored at the middle section of the MP, with its other end attached to an extension spring inside the palm. When *Servo1* loosens

ISSN: 2961-6611

Cable 1, the spring pulls the finger into an extended position. *Cable 3.1* and *Cable 3.2* form a cross wise ligament inside MP section while their ends are anchored at fingertip and PP sections. This design makes the MP-PP joint passive. As a result, fingertip, MP and PP sections can be moved in synchronously by the actuation of *Cable 1*. *Cable 4* is looped around a dowel pin on the left side of the PP, with the other end actuated by *Servo Motor 2* (*Servo 2*) located in the palm. Similarly, *Cable 5* is attached to the right side of the PP and controlled by *Servo Motor 3* (*Servo 3*). The coordinated movement of these cables and servos enables flexion-extension and circumduction around MCP joint.

The thumb's cable configuration differs slightly from the other four fingers (Fig. 3(a)-(d)). *Cables 1*, *3.1* and *3.2* function similarly to those from other fingers, controlling the flexion of the thumb. However, *Cable 2* is anchored at the middle section of the MP, with its other end attached to an extension spring (*Spring 1*) positioned parallel to the thumb. *Cable 4* is looped around the centre of PP to control flexion of this section. The extension of the PP section is regulated through the combined action of *Spring 1* and *Spring 2*. Additionally, the rotation of the CMC joint is controlled by *Cable 5* and *Spring 3*. All three servo motors (*Servo 1*, *Servo 2* and *Servo 3* for the thumb) inside the forearm control the thumb's movement.

The fingers and palm are covered with elastic silicone sheet (S840 silicone rubber) to provide friction and compliance, enhancing object grasping and manipulation. The size of the robotic hand is 10 x 16.5 x 19.8 cm (width x height x length) with weight of 0.55 kg. The size of forearm is 8.5 x 9 x 28 cm (width x height x length) with weight of 0.4 kg.

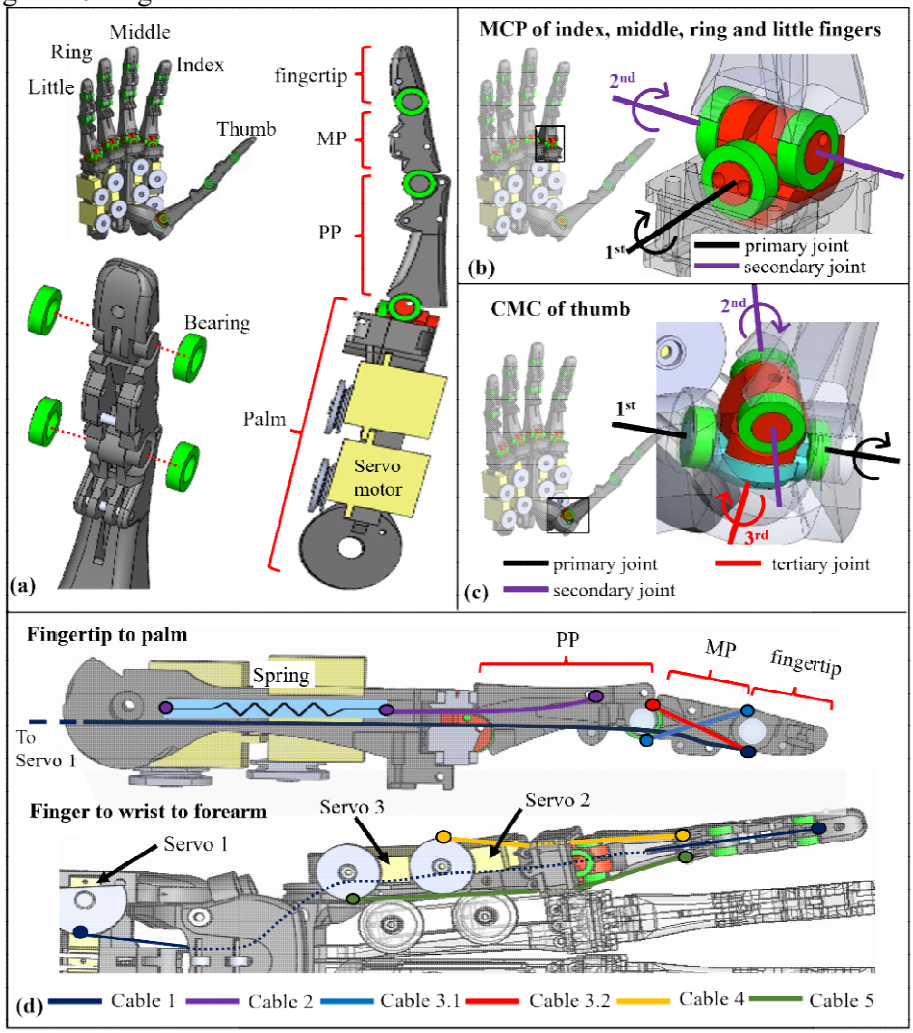

Fig. 2 Design of the robotic hand. (a) Parts of the finger. (b) Metacarpophalangeal (MCP) joint for index, middle, ring and little fingers. (c) carpometacarpal (CMC) joint of thumb. (d) cable and servo motors installation on each finger.

ISSN: 2961-6611

Vol 27, pp.67-82 Proceedings Book "Bangkok Conference - Thailand" 10.051103/PBS.251227708

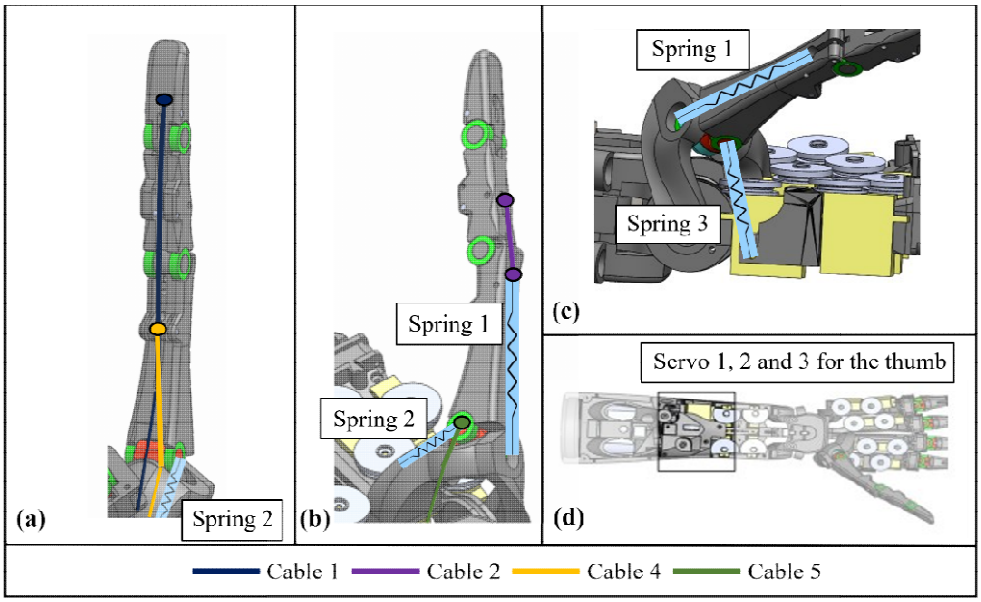

Fig. 3 Design of thumb. (a) – (c) Position of cables and springs. (d) Position of servo motors.

B. Kinematic Analysis of the Robotic Hand

A detailed understanding of the robotic hand's kinematics is crucial to precisely control its movements and replicate human-like gestures. Following the mechanical design and tendon-driven actuation described in the previous section, this section presents a comprehensive kinematic analysis of the robotic hand. The analysis establishes mathematical models that relate joint angles to fingertip positions and cable lengths, forming the basis for accurate motion planning, servo control, and workspace evaluation. These models are essential for both offline trajectory analysis and real-time teleoperation.

The control of a robotic hand primarily depends on the motion of each individual finger. Therefore, a kinematic model is established to describe the relationship between the bending angles of the fingers in 3D space and the lengths of the driving cables. The motion of a finger is analysed through three kinematic models: *i*) the finger model (Fig. 4(a)), *ii*) the circumduction model (Fig. 4(b)), *iii*) the MP model (Fig. 4(c)) and iv) the bending model (Fig. 4(d)).

The finger Model (Fig. 4(a)) describes the position of the fingertip based on the given link lengths and joint angles θ_1, θ_2, θ_3 and θ_4. In this model, θ_1 and θ_2 represent the joint angle of primary and secondary MCP joints, respectively, while θ_3 and θ_4 correspond to the joint angles of the middle phalanx (MP). and fingertip, respectively. The global coordinate frame {0} is defined at the centre of the primary MCP joint. To determine the position and orientation of the fingertip relative to the coordinate frame {0}, the transformation matrix (${}^{0}_{tip}T$) can be derived using the proximal Denavit-Hartenberg (DH) convention as followed:

$$ {}^{0}_{tip}T = \begin{bmatrix} c_1c_{234} & -c_1s_{234} & s_1 & c_1A_1 \\ s_1c_{234} & -s_1s_{234} & -c_1 & s_1A_1 \\ s_{234} & c_{234} & 0 & A_2 \\ 0 & 0 & 0 & 1 \end{bmatrix} \quad (1) $$

where $A_1 = L_1 + L_2c_2 + L_3c_{23} + L_4c_{234}$. $A_2 = L_2s_2 + L_3s_{23} + L_4s_{234}$. L_1, L_2, L_3 and L_4 are link length as shown in Fig. 4(a), s_i and c_i are sin and cos functions of θ_i, respectively, and s_{234} and c_{234} represent *sin* and *cos* functions of $(\theta_2 + \theta_3 + \theta_4)$, respectively.

The circumduction model (Fig. 4(b)) describes a conical motion about MP joint which is related among joint angles, θ_1 and θ_2 around MCP joint, and length of *Cable 4* and *Cable 5* which control motion of PP section. As shown in the Fig., both rotating angles are coupled to each other by cables. Lengths of the cable are represented by l_i, where i = 4, 5 for *Cable 4* and *Cable 5* respectively. The length of each cable l_i, is determined by its end points, one end located at point $({}^0x_i, {}^0y_i, {}^0z_i)$ with respect to the frame {0} and the other end is located at point $({}^2x_i, {}^2y_i, {}^2z_i)$ with respect to frame {2} which is attached to the secondary MCP joint. The length of cable l_i can be described as a function of θ_1, θ_2, $({}^0x_i, {}^0y_i, {}^0z_i)$ and $({}^2x_i, {}^2y_i, {}^2z_i)$ as:

ISSN: 2961-6611

Vol 27, pp.67-82 **Proceedings Book "Bangkok Conference - Thailand"** 10.051103/PBS.251227708

$$l_i = \sqrt{{B_1}^2 + {B_2}^2 + {B_3}^2} \quad (2)$$

where $B_1 = {}^2x_i\, s_2 + {}^2y_i c_2 - {}^0z_i$,
$B_2 = L_1 s_1 + {}^2x_i s_1 c_2 - {}^0y_i - {}^2y_i s_1 s_2 - {}^2z_i c_1$,
$B_3 = L_1 c_1 + {}^2x_i c_1 c_2 - {}^0x_i - {}^2y_i c_1 s_2 + {}^2z_i s_1$,
i = 4, 5.

Also, note that ${}^jx$, ${}^jy$ and ${}^jz$ are points along *x*, *y* and *z*-axis of frame {j}, respectively.

The MP model (Fig. 4(c)) describes relation between joint angles θ_3 and θ_4 for bending of finger and driving cable, *Cable 1* which controls flexion-extension of fingertip and MP sections. Based on the design of the robotic hand described in Section II.A, θ_3 and θ_4 are coupled and constrained by *Cable 3*. As a result, the mechanism between fingertip and MP sections can be considered as a cross-four bar mechanism that move together. The main constraint of the mechanism is the constant length of MP section (L_3) and length of *Cable 3.1* which locates inside MP section (l_{3M}). The relation between θ_3 and θ_4 can be derived as:

$$\theta_4 = \frac{\pi}{2} + sin^{-1}\left(\frac{r_1}{C} sin(\theta_3 + \alpha)\right) - cos^{-1}\left(\frac{{r_2}^2 + C^2 - {l_{3M}}^2}{2r_2 C}\right) \quad (3)$$

where r_1, r_2 and α are geometric dimensions of the fingers, determined based on the design and $C = \sqrt{{L_3}^2 + {r_1}^2 - 2L_3 r_1 cos(\theta_3 + \alpha)}$.

The bending model (Fig. 4(d)) describes length of *Cable 1* (l_1) as a function of joint angles θ_3 and θ_4. The length l_1 consists of two portions: l_a connecting between MP and PP sections and, l_b connecting between fingertip and MP sections. Length l_{1a} is determined from the first end on MP section (${}^2x_{a1}$, ${}^2y_{a1}$) to the second end on fingertip (${}^3x_{a2}$, ${}^3y_{a2}$). Similarly, length l_{1b} is determined from the first end on PP section (${}^3x_{b1}$, ${}^3y_{b1}$) to the second end on MP section (${}^4x_{b2}$, ${}^4y_{b2}$). Based on geometrical evaluation, l_1 can be described as:

$$l_1 = l_a + l_b \quad (4)$$

$$l_a = \sqrt{{D_1}^2 + {D_2}^2} \quad (5)$$

$$l_b = \sqrt{{D_3}^2 + {D_4}^2} \quad (6)$$

where $D_1 = L_2 + {}^3x_{a2} c_3 - {}^2x_{a1} - {}^3y_{a2} s_3$,
$D_2 = {}^3x_{a2} s_3 + {}^3y_{a2} c_3 - {}^2y_{a1}$,
$D_3 = L_3 + {}^4x_{b2} c_4 - {}^3x_{b1} - {}^4y_{b2} s_4$,
$D_4 = {}^4x_{b2} s_4 + {}^4y_{b2} c_4 - {}^3y_{b1}$.

It is noted that point (${}^2x_{a1}$, ${}^2y_{a1}$), (${}^3x_{a2}$, ${}^3y_{a2}$), (${}^3x_{b1}$, ${}^3y_{b1}$), and (${}^4x_{b2}$, ${}^4y_{b2}$) are geometric dimensions of the fingers, determined based on the design.

ISSN: 2961-6611

Vol 27, pp.67-82 Proceedings Book "Bangkok Conference - Thailand" 10.051103/PBS.251227708

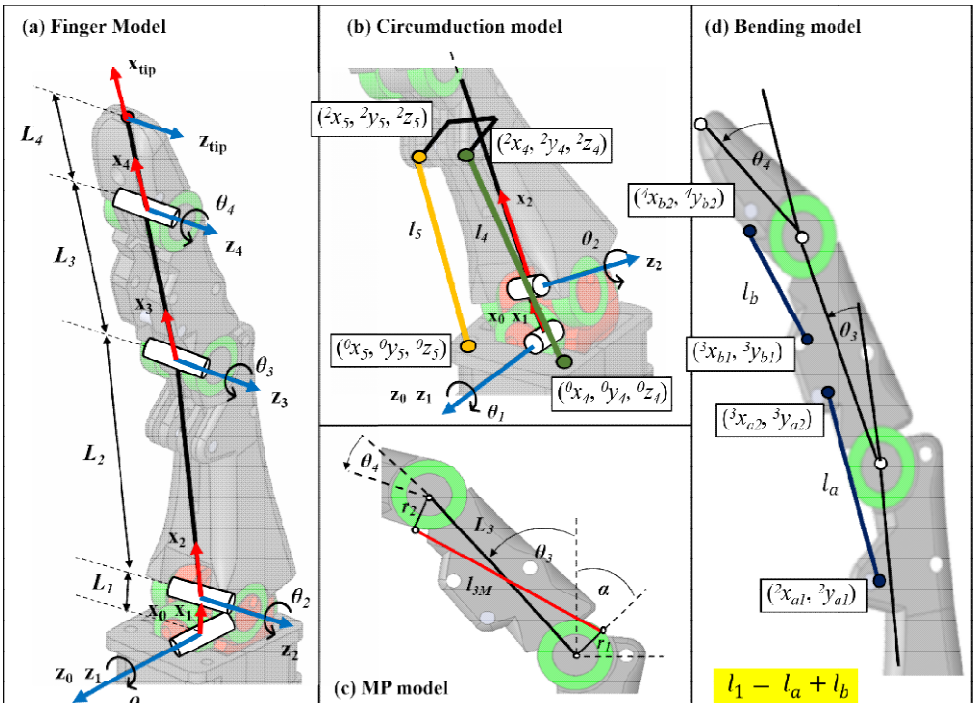

Fig. 4 Kinematic model and reachable workspace of the finger. (a) Finger model. (b) Circumduction model illustrating conical motion at MP joint. (c) MP model. (d) Bending model.

From equation (1) – (6), we can evaluate length of actuating cable (l_1, l_4 and l_5) with corresponding joint angles (θ_1, θ_2, θ_3 and θ_4) and validate reachable workspace of the finger as shown in Fig. 5(a)-(c). Joint angles are limited to the following ranges:

$$\theta_1 \in [-25°, 25°]$$
$$\theta_2 \in [0,90°]$$
$$\theta_3 \in [0,90°] \quad (7)$$

ISSN: 2961-6611

Vol 27, pp.67-82 Proceedings Book "Bangkok Conference - Thailand" 10.051103/PBS.251227708

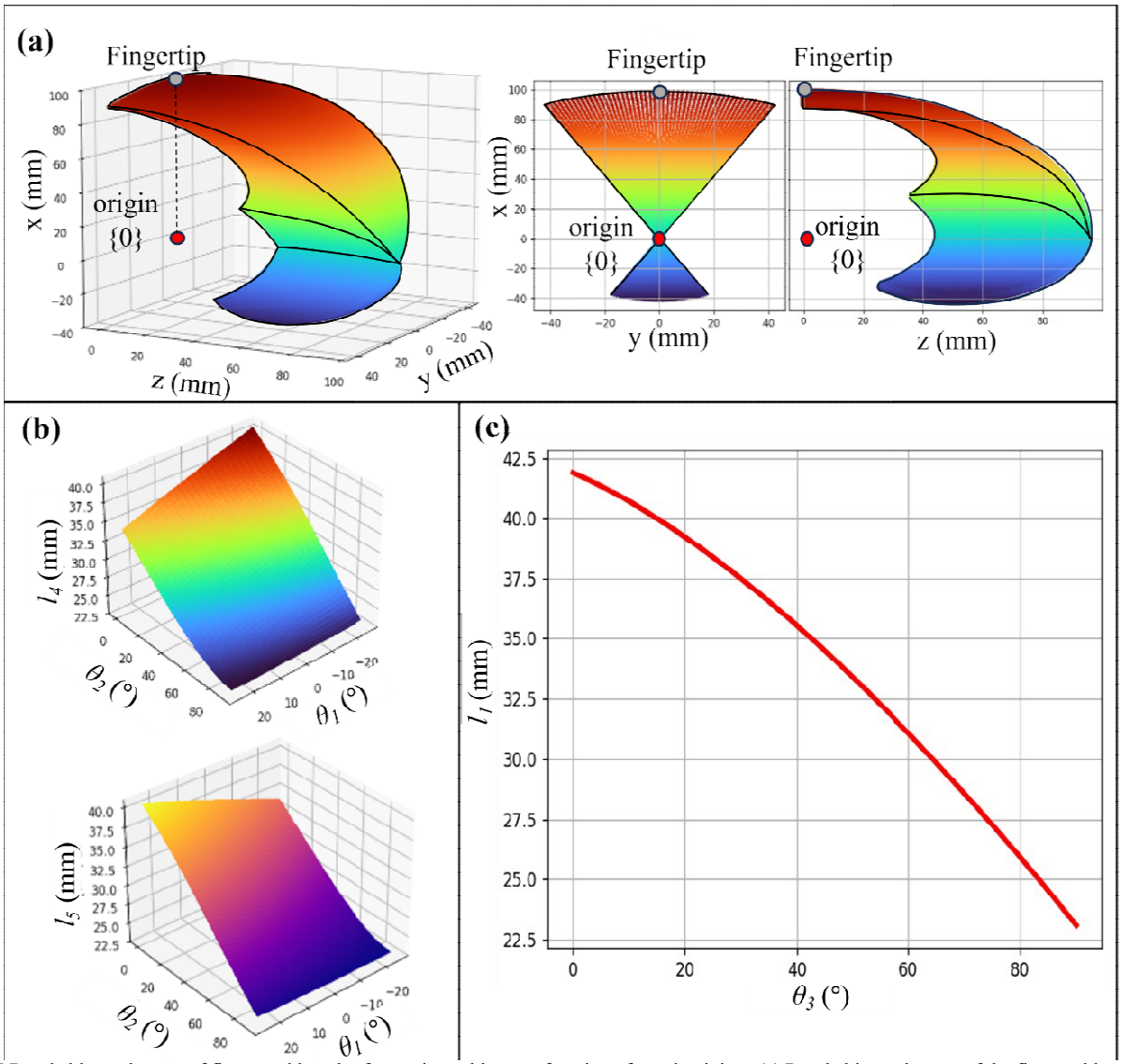

Fig. 5 Reachable workspace of finger and length of actuating cables as a function of rotating joints. (a) Reachable workspace of the finger with respect to global coordinate. (b) Length of *Cable 4* (top) and *Cable 5* (bottom) as a function of θ_1 and θ_2. (c) Length of *Cable 1* a function of θ_3.

Fig. 5(a) illustrates the reachable workspace of the finger, derived from the geometric parameters of the index finger. All points on and within this surface correspond to fingertip positions relative to the primary MCP joint axis, defined as the origin of frame {0}. The resulting workspace exhibits a close resemblance to that of a human finger, as reported in previous studies [22]. The workspace below the MCP joint is relatively small. Fig. 5(b) illustrates the lengths of *Cable 4* (l_4) and *Cable 5* (l_5) as functions of the rotation angles θ_1 and θ_2. Achieving any desired angular configuration (θ_1 and θ_2) requires that the corresponding values of l_4 and l_5 simultaneously satisfy the constraints depicted in the plot. Fig. 5(c) depicts the length of *Cable 1* (l_1) as a parabolic function of θ_3 for finger bending motion. From the analysis, all rotating angles and motion of finger is fully controlled by adjusting length l_1, l_4 and l_5. With known diameter of pulley, displacement of servo motors to achieve required length of cable can be calculated.

C. Design of the Flex Sensor-Based Glove for Real-Time Control

To achieve intuitive and accurate teleoperation of the robotic hand, a sensor interface that can effectively capture human finger motion is essential. Building upon the kinematic models established in the previous section, which define the relationship between joint angles and cable lengths, we developed a flex sensor-based glove to enable real-time control of a robotic hand, as shown in Fig. 6(a). The glove features nine 2.2-inch flex sensors. Each of the index, middle, ring, and little fingers is fitted with two flex sensors to measure

ISSN: 2961-6611

finger flexion and extension. The first sensor is positioned at the upper part of the finger covering from the fingertip to the end of the proximal phalanx (PP) to capture bending in this section, while the second sensor covers lower part of the finger from the PP to the palm to measure movement at the PP-palm joint. In contrast, the three active joints of the thumb are controlled using a single flex sensor. The flex sensors are attached to the glove using Velcro tape, which is slotted through loops of sewing thread. This design allows the sensors to shift slightly during maximum finger flexion and extension, preventing excessive strain and ensuring accurate motion tracking. The readings from each flex sensor are finely calibrated and mapped to the corresponding servo motor rotation angles, ensuring precise finger movement replication. To enhance the accuracy of the flex sensor readings, the glove is designed without additional electrical components, a microcontroller, or a power supply.

D. Design of the Flex Sensor-Based Glove for Real-Time Control

The robotic hand consists of 15 servo motors (ES3301). Eight of these motors are positioned in the palm to control the flexion, extension, and circumduction of the MCP joint, while the remaining seven are housed within the forearm to regulate the flexion and extension of the fingertip-to-PP section. All servo motors are connected to two 16-channel servo motor drivers (PCA9685 PWM driver IC), both positioned at the end of the forearm. The first driver controls the first eight servo motors, while the second manages the remaining nine. The drivers are powered by a 5V supply with a maximum current of 10A from the electronic box. Their output ports are linked to the microcontroller (Arduino Mega 2560), located in the electronic box, via I2C communication. Flex sensors of the glove are also wired to the electronic box which are then connected to analog-input pins of the microcontroller. The microcontroller is powered by an external computer via a USB port and communicates with the computer through a serial connection. This enables real-time transmission of sensor readings and the operational status of the robotic hand, ensuring continuous monitoring and precise control during operation. The control architecture of the proposed system is illustrated in Fig. 6(b) comprising of three components: *i*) Servo motors and drivers within the robotic hand, *ii*) A flex sensor-based glove, and iii) A electronic box that processes data between the robotic hand and glove while supplying power to both.

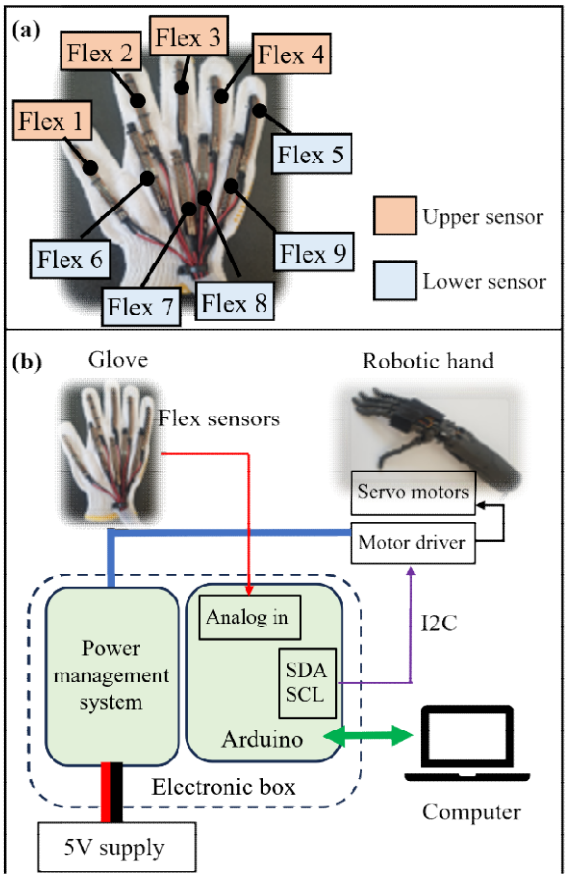

ISSN: 2961-6611

Fig. 6 The design of glove and control system. (a) The flex sensor-based glove for real-time control. (b) simplified block diagram of control system and electronic box.

III. Performance Evaluation

With the mechanical structure of the robotic hand and the flex sensor-based glove established, it is essential to validate the system's effectiveness through experimental evaluation. This section presents the performance assessment of both the flex sensor-based glove and the integrated robotic hand system under various operating conditions. The goal is to verify the glove's sensing accuracy, repeatability, and responsiveness, as well as the robotic hand's ability to replicate human finger motions and perform complex manipulation tasks.

A. Performance of Flex Sensor-based Glove

The proposed flex sensor-based glove has been developed. To evaluate its performance, the glove is worn by the user to simulate realistic conditions. Flex sensor readings are recorded under both static and dynamic conditions. In Fig. 6(a), the glove incorporates nine flex sensors. The first five sensors, labelled Flex 1 to Flex 5, are positioned on the upper portions of each finger to capture bending from the fingertip to the PP sections. The remaining four sensors, labelled Flex 6 to Flex 9, are placed at the lower portion of fingers, covering from the PP sections and the palm of the index, middle, ring, and little fingers to measure bending in those areas. To minimize sensor noise and smooth the signal, complementary filter with a filter coefficient α=0.45 was applied to the program.

The results of the static test are presented in Fig. 7(a) showing a linear relation between analog reading value from the sensor and bending angle. The reading value of Flex 1 to Flex 5 and Flex 6 to Flex 9 were obtained by bending MP joint (θ_3) and PP joint (θ_1), respectively. As observed from the plot, all sensors show different initial reading value at 0^o and sensitivity. At 0^o and 90^o, the sensor reading can be varied from 0 to 35.5 and 106.8 to 227.2, respectively (analog reading value from the sensor is unitless.). Flex sensors located at the upper portion tend to have higher reading value and sensitivity than those of lower portion. This variation is a result of different length of finger that each sensor covers.

The results of the dynamic test are shown in Fig. 7(b). In this test, the user's hand, equipped with the glove, repeatedly performs 5-second fully opening and 5-second closing hand postures in a periodic pattern. Hand opening and closing correspond to $\theta_1 = \theta_3 = 0^o$ and $\theta_1 = \theta_3 = 90^o$, respectively. Similar to the static results, each sensor exhibits different initial and terminal reading values. For the sensors positioned on the upper portion of the hand (Flex1 to Flex5), the readings during hand opening increase progressively with each cycle. In the first cycle, the sensor readings ranged from 0 to 14.29, but by the third cycle, they shifted to between 21.25 and 36.27. In contrast, the readings from the lower portion sensors (Flex6 to Flex9) remained stable, varying by less than ±3% of its full-scale reading throughout the cycles. Comparing the characteristics of upper and lower sensors, the upper sensors show greater fluctuations due to a rigidity of sensor. Unlike flex sensor, a finger bends into any configuration, the wrinkled skin at the knuckles stretches to accommodate the movement, preventing skin damage. Although the flex sensors bend along with the finger, their length remains constant. As a result, the flex sensors do not fully return to their initial shape during cyclic movements, leading to gradual deformation and shift in their readings over time.

ISSN: 2961-6611

Vol 27, pp.67-82 Proceedings Book "Bangkok Conference - Thailand" 10.051103/PBS.251227708

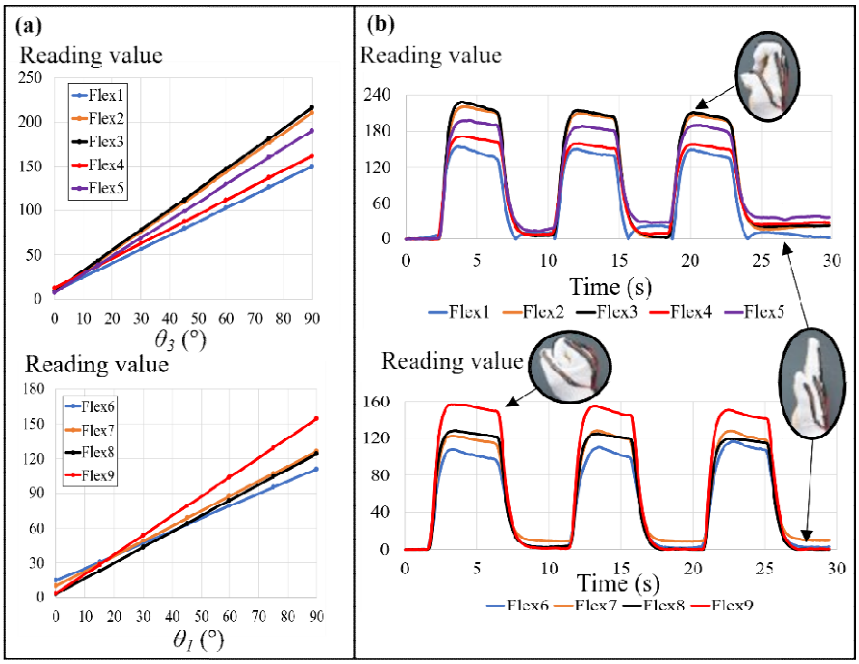

Fig. 7 Performance of the flex sensor-based glove. Sensor reading value under (a) static condition (n = 5 for each data point) and (b) dynamic condition.

B. Finger Motion

Following the evaluation of the flex sensor-based glove under both static and dynamic conditions, the next step is to examine how accurately the robotic hand replicates human finger movements based on the glove's sensor inputs. This section demonstrates the motion capabilities of the robotic finger, driven by the tendon-actuated mechanism in response to real-time flex sensor data. By analysing the individual and coordinated joint behaviours, we validate the effectiveness of the glove-hand interface in reproducing complex and natural finger motions.

Fig. 8 illustrates the motion of a finger controlled by a flex sensor-based glove. The dexterity of the finger is demonstrated in Supplementary Video S1. The entire finger, from the fingertip to the proximal phalanx (PP) section, can bend around the secondary MCP joint (θ_2) by adjusting the lengths of l_4 and l_5 to be equal as shown in Fig. 8(a). Fingertip and MP section can be rotated independently from PP section by adjusting the length l_1 (corresponding to θ_3 and θ_4) as shown in Fig. 8(b). Both rotations have a maximum stroke of 90° and allow the entire finger to reach any point in workspace on its x_0-y_0-z_0 plane. Movement in spatial workspace (x_0-y_0-z_0 plane) and circumduction can be easily achieved by adjusting l_4 and l_5 to be different (Fig. 8(c)). The synchronization between robotic hand and the glove is demonstrated in Supplementary Video S2.

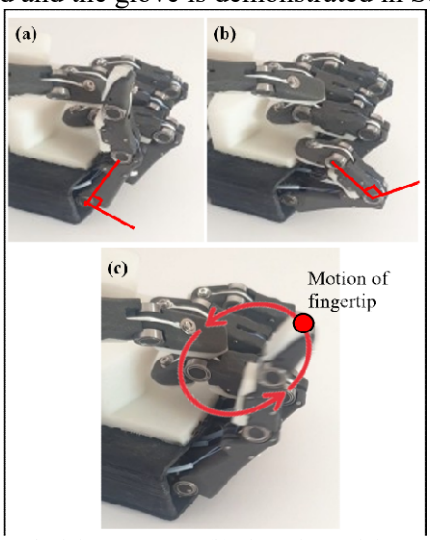

Fig. 8 Finger Motion. (a) PP-palm joint movement. (b) Fingertip-MP joint movement. (c) Circumduction.

ISSN: 2961-6611

C. Manipulation Test of the Robotic Hand

While the individual finger motions highlight the dexterity and range of movement enabled by the tendon-driven mechanism and flex sensor-based control, it is equally important to assess the system's performance in real-world manipulation tasks. To this end, a series of manipulation experiments were conducted using the fully integrated system, in which the robotic hand—teleoperated via the flex sensor-based glove—interacted with a variety of objects differing in shape and size. These tests serve to validate the system's practical effectiveness in achieving stable grasps, executing coordinated finger movements, and handling objects under dynamic control conditions.

To evaluate these capabilities, the robotic hand was tasked with grasping and manipulating various objects, as illustrated in Fig. 9. The initial experiments involved items with simple geometries, including a spherical ball, a cylindrical object, and a mug (Fig. 9(a); see also Supplementary Video S3). In each case, the robotic fingers successfully enclosed the objects, maintaining stable and secure grasps—even when the robotic arm underwent motion during the manipulation process.

Notably, the robotic hand was able to grasp the mug in a manner closely resembling a natural human grip, effectively demonstrating the advantage of using the glove. As shown in Fig. 9(b), the robotic hand is also capable of grasping and holding tiny objects, such as a needle, using the tips of the index finger and thumb (see Supplementary Video S4).

With the addition of a supporting palm, the robotic hand can grasp and hold objects more securely. As shown in Fig. 9(c), it can hold and lift a 2.1 kg hammer by positioning the handle against its palm (see Supplementary Video S5). Unlike the earlier demonstration in Fig. 9(a), where objects were held primarily using fingertip force, the robotic hand in this scenario employs compressive force between its five fingers and the palm to maintain the hammer's orientation. The proposed robotic hand can also hold and manipulate simple tools, as demonstrated in Fig. 9(d), where it operates a wire stripper. In this demonstration, the robot uses its thumb and palm to stably grasp the tool while the remaining four fingers operate the tool (see Supplementary Video S6). Lastly, the versatility of using the glove to control the motion of the robotic hand was demonstrated by successfully picking up and holding a marker pen (Fig. 9(e); see also Supplementary Video S7). In this experiment, the marker pen was initially placed on the floor. The robotic hand manipulated its fingers to grasp and secure the pen in its palm, despite the limited contact area. Notably, the pen was oriented appropriately, enabling it to be used in subsequent tasks.

ISSN: 2961-6611

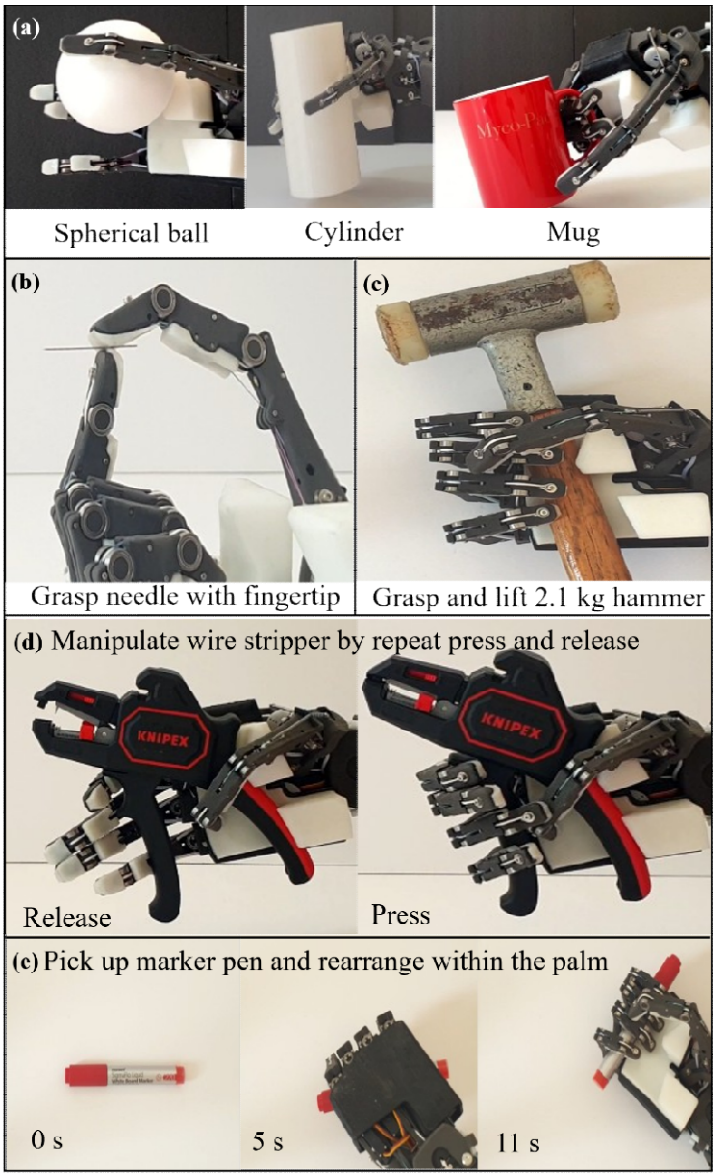

Fig. 9 Demonstration of the robotic hand with flex sensor-based glove. (a) Grasping simple objects including spherical ball, cylinder and mug. (b) Grasping needle. (c) Grasping and lifting 2.1 kg hammer. (d) Manipulating wire stripper by repeat press and release. (e) Picking up marker pen and rearrange within the palm.

IV. CONCLUSION

This study presented the design, development, and evaluation of a tendon-driven robotic hand system controlled via a flex sensor-based glove for complex object grasping and manipulation. The robotic hand, inspired by human anatomy, features 15 active degrees of freedom and a tendon-driven mechanism that enables dexterous motion of each finger. The mechanical design replicates key human joint functions, particularly the MCP and CMC joints, allowing for precise finger articulation, circumduction, and spatial manipulation. Covered with a silicone layer, the hand achieves enhanced grip compliance and friction, enabling it to interact effectively with real-world objects. The size of the robotic hand is 10 x 16.5 x 19.8 cm (width x height x length) with weight of 0.55 kg. The size of forearm is 8.5 x 9 x 28 cm (width x height x length) with weight of 0.4 kg.

To control this robotic hand in real time, a wearable glove equipped with nine flex sensors was developed. The glove captures human finger movements and translates them into motor commands through a lightweight, low-latency control system. Both static and dynamic tests confirmed the glove's responsiveness, stability, and sensor fidelity, with clear mapping between sensor readings and joint angles.

ISSN: 2961-6611

Comprehensive manipulation tests demonstrated the system's capability to perform a wide range of tasks, from grasping geometric objects and delicate tools (e.g., a needle or wire stripper) to handling heavy and irregular items like a 2.1 kg hammer. The hand's ability to adapt its grip through coordinated finger and palm interaction closely mimics human strategies, including fingertip manipulation, palm-supported grasps, and in-hand object manipulation.

These results confirm that the integration of a flex-sensor glove with a tendon-driven robotic hand enables intuitive and effective teleoperation for complex tasks. This work contributes to the field of human-robot interaction by offering a practical, real-time control solution and a versatile robotic platform. Future research may extend this system with tactile feedback, autonomous control modes, wrist articulation and improvement of flex sensor-based glove for better controllability of MCP and CMC joint to further improve its manipulation capabilities and usability in service robotics, prosthetics, and teleoperation applications.

MULTIMEDIA LINK

Video S1: Finger movement
The video demonstrates dexterity of the finger including finger bending and circumduction.
Link: https://vimeo.com/1085170062/e616b94751

Video S2: Teleoperation of robotic hand via flex sensor-based glove
This video demonstrates the synchronization between robotic hand and the glove.
Link: https://vimeo.com/1085170502/a0b5f7d69e

Video S3: Grasping objects with fingers
This video shows the initial tests involving objects with simple geometries, including a spherical ball, cylinder, and mug.
Link: https://vimeo.com/1085171146/a116f4fbca

Video S4: Grasp sewing needle
This video shows the robotic hand capable of grasping and holding tiny objects, such as a needle, using the tips of the index finger and thumb.
Link: https://vimeo.com/1085171167/8fdf137ce4

Video S5: Grasp and lift 2.1kg-hammer
This video shows the robotic hand capable of grasping and lifting a 2.1 kg hammer by positioning the handle against its palm.
Link: https://vimeo.com/1085171175/dff8d4cff3

Video S6: Manipulating wire stripper
The proposed robotic hand can hold and manipulate simple tools where it operates a wire stripper. In this demonstration, the robot uses its thumb and palm to stably grasp the tool while the remaining four fingers operate the tool.
Link: https://vimeo.com/1085171196/800169a91d

Video S7: Pick up marker and regrasp within the palm
The versatility of using the glove to control the motion of the robotic hand was demonstrated by successfully picking up and holding a marker pen.
Link: https://vimeo.com/1085171235/33de193f32

CONFLICT OF INTEREST

The authors declare no conflict of interest.

REFERENCES

[1] G. P. Kontoudis, M. Liarokapis, K. G. Vamvoudakis, *et al.*, "An adaptive actuation mechanism for anthropomorphic robot hands," *Frontiers in Robotics and AI*, vol. 6, pp. 47–62, 2019.
[2] T. Hao, H. Xiao, J. Wang, *et al.*, "Friction enhancement through fingerprint-like soft surface textures in soft robotic grippers for grasping abilities," *Tribology Letters*, vol. 72, no. 2, pp. 47–58, 2024.
[3] C. Piazza, G. Grioli, M. G. Catalano, *et al.*, "A century of robotic hands," *Annu. Rev. Control Robot. Auton. Syst.*, vol. 2, no. 1, pp. 1–32, 2019.
[4] E. Nazma and S. Mohd, "Tendon driven robotic hands: A review," *Int. J. Mech. Eng. Robot. Res.*, vol. 1, no. 3, pp. 350–357, 2012.
[5] J. Butterfaß, M. Grebenstein, H. Liu, *et al.*, "DLR-Hand II: Next generation of a dexterous robot hand," in *Proc. IEEE Int. Conf. Robot. Autom. (ICRA)*, vol. 1, pp. 109–114, 2001.

ISSN: 2961-6611

[6] J. Best and A. Fakhari, "Development of a novel impedance-controlled quasi-direct-drive robotic hand," *arXiv preprint*, arXiv:2405.18730, pp. 18730–18737, 2024.
[7] G. Li, X. Liang, Y. Gao, T. Su, Z. Liu, *et al.*, "A linkage-driven underactuated robotic hand for adaptive grasping and in-hand manipulation," *IEEE Trans. Autom. Sci. Eng.*, 2023.
[8] M. Cheng, L. Jiang, and Z. Liu, "Design and optimization of an anthropomorphic robot finger," *Biomimetics*, vol. 10, no. 3, pp. 170–186, 2025.
[9] U. Kim, D.-H. Lee, Y. B. Kim, *et al.*, "S-Surge: Novel portable surgical robot with multiaxis force-sensing capability for minimally invasive surgery," *IEEE/ASME Trans. Mechatronics*, vol. 22, no. 4, pp. 1717–1727, 2017.
[10] U. Kim, D. Jung, H. Jeong, *et al.*, "Integrated linkage-driven dexterous anthropomorphic robotic hand," *Nature Commun.*, vol. 12, no. 1, pp. 7177–7189, 2021.
[11] S. Shirafuji, S. Ikemoto, and K. Hosoda, "Development of a tendon-driven robotic finger for an anthropomorphic robotic hand," *Int. J. Robotics Res.*, vol. 33, no. 5, pp. 677–693, 2014.
[12] X. Deng, S. Weirich, R. K. Katzschmann, *et al.*, "A rapid and robust tendon-driven robotic hand for human-robot interactions playing rock-paper-scissors," in *Proc. 2024 IEEE Int. Conf. Robot. Human Interact. Commun.*, pp. 2347–2354, 2024.
[13] A. Suebsomran, "Development of robot gripper and force control," in *Proc. 13th World Congr. Intell. Control Autom. (WCICA)*, pp. 433–437, 2018.
[14] P. Weber, E. Rueckert, R. Calandra, *et al.*, "A low-cost sensor glove with vibrotactile feedback and multiple finger joint and hand motion sensing for human-robot interaction," in *Proc. 2016 IEEE Int. Symp. Robot. Human Interact. Commun. (RO-MAN)*, pp. 99–104, 2016.
[15] S. Zhu, A. Stuttaford-Fowler, A. Fahmy, *et al.*, "Development of a low-cost data glove using flex sensors for the robot hand teleoperation," in *Proc. 2021 Int. Symp. Robot. Intell. Manuf. Technol. (ISRIMT)*, pp. 47–51, 2021.
[16] K. Oka, Y. Sato, and H. Koike, "Real-time fingertip tracking and gesture recognition," *IEEE Comput. Graph. Appl.*, vol. 22, no. 6, pp. 64–71, 2002.
[17] J. L. Raheja, R. Shyam, U. Kumar, *et al.*, "Real-time robotic hand control using hand gestures," in *Proc. 2nd Int. Conf. Mach. Learn. Comput.*, pp. 12–16, 2010.
[18] Y. Sun, J. Falco, M. A. Roa, *et al.*, "Research challenges and progress in robotic grasping and manipulation competitions," *IEEE Robot. Autom. Lett.*, vol. 7, no. 2, pp. 874–881, 2021.
[19] R. Knight, "DexHand – An Open Source Dexterous Humanoid Robot Hand," [Online]. Available: https://www.dexhand.org/, 2024.
[20] V. K. Nanayakkara, G. Cotugno, N. Vitzilaios, *et al.*, "The role of morphology of the thumb in anthropomorphic grasping: A review," *Front. Mech. Eng.*, vol. 3, p. 5, 2017.
[21] [21] S. W. Byun and S. P. Lee, "Implementation of hand gesture recognition device applicable to smart watch based on flexible epidermal tactile sensor array," *Micromachines*, vol. 10, no. 10, p. 692, 2019.
[22] U. K. Alam, K. Shedd, and M. Haghshenas-Jaryani, "Trajectory control in discrete-time nonlinear coupling dynamics of a soft exo-digit and a human finger using input–output feedback linearization," *Automation*, vol. 4, no. 2, pp. 164–190, 2023.

ISSN: 2961-6611